Characterisation of thermal barrier sensor coatings synthesised by sol–gel route

Lisa Pin [a,b,*], Christopher Pilgrim [c,d], Jörg Feist [c,d], Yannick Le Maoult [a], Florence Ansart [b], Philippe Lours [e]

[a] University of Toulouse, Mines Albi – Institut Clément Ader, Campus Jarlard, F-81013 Albi Cedex 09, France
[b] University of Toulouse, UPS-INP-CNRS, Institut Carnot CIRIMAT, 118 Route de Narbonne, 31062, Toulouse, Cedex 09, France
[c] Imperial College London, London SW7 2AZ, UK
[d] Sensor Coating Systems, Imperial Incubator, Imperial College, London SW7 2AZ, UK
[e] Université de Toulouse Mines Albi Institut Clément Ader, 81 013 Albi, France

ABSTRACT

Further improvements in the efficiency of gas turbines are recognised to come from increases in turbine entry temperatures. Accurate temperature measurements are crucial to achieve these increases whilst maintaining reliability and economic component life. The combination of phosphor thermometry and thermal barrier coating (TBC) technology has led to the development of functional temperature sensor coatings which have several advantages over conventional temperature measurement techniques. Developments in sol–gel processing indicate that this method could be used for the production, or particularly, the repair of TBCs in the future.

This paper demonstrates, for the first time, that sol–gel processing can be used to make sensor TBCs. The optimum concentration of $SmO_{1.5}$ was 2 wt.% in YSZ to achieve the brightest phosphorescence emission. Above this concentration the overall intensity of the emission reduces and the transitions from $^4F_{3/2}$ were suppressed. Furthermore, a similar suppression of these transitions was observed when the product of the sol–gel was heat treated to 1100 °C. This was concluded to be due to a higher degree of crystallinity allowing a greater interaction between the dopant ions. The dependence of the phosphorescence spectrum on heat treatment temperature provides the first indication that YSZ produced through sol–gel could be used to detect historic temperatures.

An evaluation of the subsurface measurement and temperature capabilities has shown that the phosphorescence can be detected from relatively thin layers, 20 μm, even under 50 μm of undoped YSZ coating. Although the temperature detection range, 400–700 °C, is too low for advanced TBCs the material could be used in low temperature regimes or for health monitoring purposes.

1. Introduction

Thermal barrier coatings (TBCs) have become an integral part of high performance gas turbine engines. These multilayer coating systems enable the firing temperature of the turbine to increase and hence improve efficiency of operation while also maintaining practical component life. However the ongoing drive for greater efficiencies is recognised to come from further increases in temperature [1,2]. As an approximation a 50 °C increase in turbine entry temperature (TET) will cause a significant gain in efficiency [3]. However, the same temperature increase at the TBC/substrate interface can cause a sixfold decrease in TBC service life [4]. It is, therefore, critical to obtain accurate temperature measurements

on the coated surface and at the substrate interface to safely achieve efficiency increases. Conventional temperature measurement methods, such as pyrometry or thermocouples, have intrinsic disadvantages when employed to measure coating temperatures. Changes in emissivity of the coating, reflections from the combustion environment and glowing particles in the gas flow all cause errors in pyrometer measurements. Thermocouples and fibre optic sensors have limited applicability due to their intrusive nature, particularly for rotating components. Thermal barrier sensor coatings (TBsCs) have been conceived to overcome these disadvantages [5]. These coatings integrate optically active material into the TBC to perform phosphor thermometry using a functional TBC, allowing remote temperature measurements inside the coating. Furthermore the sensor layer can be placed at different positions through the thickness of the coating enabling temperature and heat flux measurements in the coatings [6,7].

The first ever application of such a TBC sensor system for temperature detection on an operating gas turbine was successfully demonstrated in October 2010 by some of the co-authors, using

* Corresponding author at: University of Toulouse, Mines Albi – Institut Clément Ader, Campus Jarlard, F-81013 Albi Cedex 09, France. Tel.: +33 5 63 49 32 82; fax: +33 5 63 49 61 63.

E-mail address: lisa.pin@mines-albi.fr (L. Pin).

a Rolls-Royce jet engine [8–10]. The measurements, performed under several different operating conditions on a nozzle guide vane, the combustor liner and turbine blades, show better performance than applied pyrometers. A video demonstration of the engine measurements can be found under [11].

Two main processes are used to apply TBCs to components, Air Plasma Spray and Electron Beam Physical Vapour Deposition (EB-PVD) [12]. The successful implementation of TBsCs has been demonstrated for both of these deposition methods [6,13]. Sol–gel processing, however, has gained increasing credibility over recent years for the production of coatings with non-directional porosity because it offers benefits in processing costs and flexibility, and the potential to repair damaged TBCs [14–16]. Using this method it is possible to produce multi-layered TBCs with control over the thickness, depth and concentration of dopants in each layer. Furthermore, the advances in the processing by some of the co-authors have demonstrated the durability of sol–gel coatings under cyclic oxidation at 1100 °C [17]. Hence, the objective of the present paper is to solely investigate the use of sol–gel to produce sensor TBCs for phosphor thermometry measurements with samarium as the active dopant. Firstly, the optimum dopant concentration is determined for samarium in an yttria stabilised zirconia (YSZ) host. Secondly, this material is integrated into a YSZ bulk coating at different depths to evaluate the effectiveness of embedding the sensor layer. Finally, the decay lifetime of the phosphorescence is recorded over a range of temperatures to establish its working limits for detection.

2. Theoretical aspects

By introducing rare earth elements into the YSZ host the material becomes luminescent. The rare earth ions are embedded within the crystal structure and act as optically active centres. These elements are widely used as luminescent activators because their optical properties are largely dictated by electron energy state transitions in the partially filled 4f shell which is surrounded by the outer 5d and 6s shells which provide the bonding with the host lattice. As a result the host material has minimal, albeit meaningful, influence on the optical transitions of the rare earth ion. Consequently when the dopant levels are sufficiently low, below a few percent, the ions are isolated and can be considered free. The allowed energy levels correspond to distinct peaks in the emission spectrum. The defined spectral emission enables the luminescence to be distinguished from background radiation making measurements at high temperatures possible [18].

The luminescence is affected by temperature in several ways [19]. The change in the temporal characteristics, however, is most often exploited for phosphor thermometry. After pulsed excitation the electrons return to the ground state by radiative and non-radiative processes. In radiative processes the electrons release photons, or light, and in non-radiative processes the energy is released as phonons, or lattice vibrations. It is well known that the decay of the phosphorescence, I, with time, t, can be written as in Eq. (1), where I_0 is the intensity at $t = 0$ and τ is the decay time.

$$I(t) = I_0 \exp\left(-\frac{t}{\tau}\right) \tag{1}$$

The transition probability, however, is the sum of the radiative and non-radiative decay rates, and so the lifetime decay of the phosphorescence can be expressed as in Eq. (2), where P_R and P_{NR} are the probability of radiative and non-radiative transitions respectively.

$$\tau = \frac{1}{P_R + P_{NR}} \tag{2}$$

Unlike the radiative decay rate, the non-radiative decay rate is dependent on temperature. As the temperature increases more phonons are available for multi-phonon relaxation hence increasing the probability of non-radiative decay. Higher temperatures, therefore, result in faster decay times.

The temperature dependency of the non-radiative transitions can be obtained by the theory of multi-quantum emissions [20], given in Eq. (3) where n corresponds to the number of phonons emitted with an energy of E_{phonon}, k_B is the Boltzmann constant and T is the absolute temperature. This equation can be used to predict the change in phosphorescence decay with temperature. The relationship shows that at low temperatures the non-radiative decay is almost constant however the decay becomes increasingly faster at higher temperatures. The transition between these two regimes is typically referred to as quenching temperature and denotes the minimum temperature of the phosphor sensitivity range.

$$P_{NR}(T) = P_{NR}(T = 0)\left[1 - \exp\left(\frac{E_{phonon}}{k_B T}\right)\right]^{-n} \tag{3}$$

3. Experiments

3.1. Synthesis of YSZ:Sm powder

Batches of YSZ (9.7 mol% $YO_{1.5}$) were produced with 1, 2 and 5 wt.% $SmO_{1.5}$ using the sol–gel method. The precursors for the sol were zirconium(IV) propoxide ($Zr(OPr)_4$) (Aldrich), yttrium(III) nitrate hexahydrate (Acros Organics), samarium(III) nitrate hexahydrate (Acros Organics), and 1-propanol was used as the solvent. To reduce the hydrolysis rate of the zirconium alcoxyde, acetylacetone (AcAc) was used as a complexing agent [21]. The volume rates of $[AcAc/Zr(OPr)_4]$ and $[H_2O/Zr(OPr)_4]$ were kept constant at 0.8 and 9.5 respectively.

The YSZ sol was reduced to a gel by heating at 50 °C in a drying oven for 12 h. A further drying technique, described in more detail elsewhere [15], was used to produce a gel referred to as aero-gel. The technique involved drying the sol at supercritical conditions for the solvent and is reported to have favourable properties for the production of YSZ dip coatings [15]. The sol was placed in an autoclave (Parr Instrument, 160 mL) where it was maintained at 270 °C and 51 bar for 2 h. In the final hour the solvent was slowly released from the chamber and the autoclave was cooled to room temperature. Two different batches were produced from the resultant product, one batch was heated at 700 °C for 2 h, the other at 950 °C for 2 h.

3.2. Synthesis of multi-layered coatings

Multi-layered coatings, containing both YSZ and YSZ:Sm layers, were produced by slurry dipping. The slurry was a composite of sol–gel synthesised powders combined with precursor sol. This method was used in order to achieve a coating thickness similar to that used in TBC applications [14]. The two different materials were deposited using two slurries, one of YSZ and another of YSZ:Sm with a $SmO_{1.5}$ concentration of 2 wt.%. The slurries were formed by dispersion of the powder batch heated to 700 °C in sol of the same composition. The substrates, nickel based superalloy with an aluminised bond-coat, were dipped into the slurry to form the desired layer, then withdrawn at a controlled speed of 250 mm/min to ensure an even coating surface. Previous calibration work has shown that the coating thickness is controlled by the slurry viscosity and withdrawal speed, which were set to produce approximately 10–20 μm thick layers in one dip procedure.

Three coating constructions were produced as illustrated in Fig. 1. A YSZ:Sm layer, approximately 20 μm thick, was produced at
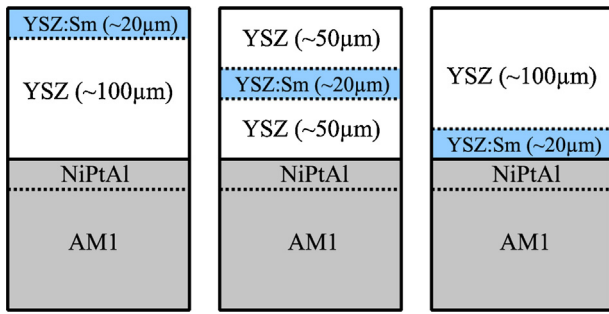
Fig. 1. A schematic of the three different multi-layered coating samples where the doped layer is at the surface (left), in the middle (centre) and at the bond coat interface (right).

three different positions in three samples of an otherwise 100 μm thick undoped YSZ coating. The coatings were then heat treated at 1100 °C for 2 h with a gradual heating and cooling rate of 50 °C/h to minimise stresses due to the difference in thermal expansion between the substrate and the coatings.

3.3. Materials characterisation

To verify that the synthesised material was produced in the desired tetragonal phase, structural analysis was conducted by X-ray diffraction (XRD) and analysed using the Rietveld method [22]. The XRD traces were collected at room temperature by scanning the angular range from 20° to 100° with a Brucker AXS D4 diffractometer. Copper radiation was used as the X-ray source ($\lambda(CuK\alpha1) = 1.5406\,Å$; $\lambda(CuK\alpha2) = 1.5445\,Å$) and filtered with a nickel filter. The peak identification was conducted whereby the observed XRD trace was fitted to the calculated trace using a least squares routine. For the tetragonal phase, the space group used for Rietveld refinement was P42/*nmc* (137).

3.4. Phosphorescence characterisation

The phosphorescence from the powder and coatings was measured at ambient and high temperature. The excitation of the phosphorescence was the same in both cases. A Nd:YAG laser (Brilliant B, Quantel), frequency quadrupled to operate at 266 nm with a pulse frequency, duration and energy of approximately 10 Hz, 5 ns and 40–50 mJ respectively, was directed at the sample using a single mirror. In the ambient temperature measurements the emission spectrum of the phosphorescence was recorded. The emission was imaged onto the entrance slit of a spectrometer (Horiba Jobin Yvon, MicroHR) using a varifocal lens, as shown in Fig. 2. The spectrometer delivered the light to a pre-calibrated CCD array (Horiba Synature)
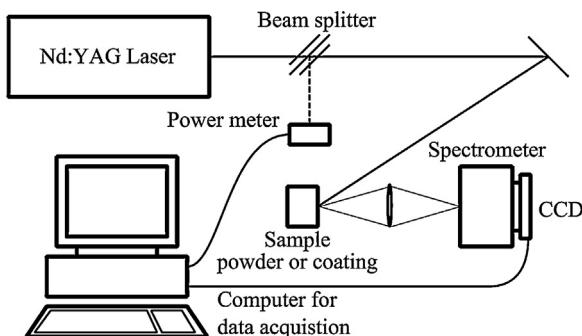

Fig. 2. Experimental setup used to measure the phosphorescence emission spectrum at ambient temperature.
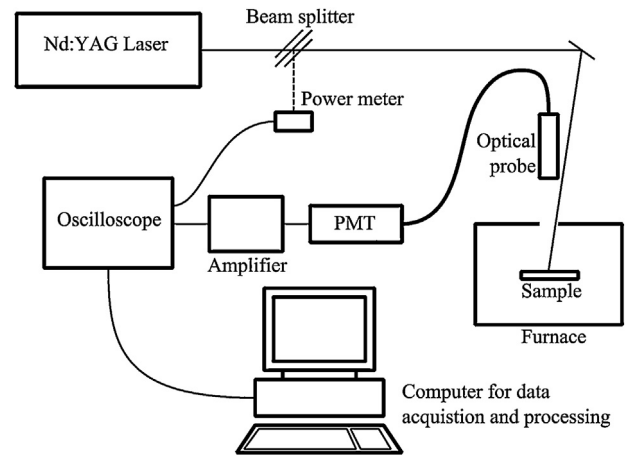

Fig. 3. Experimental setup used to measure the phosphorescence emission decay lifetime at elevated temperatures.

for an exposure time of three seconds. The digitised signal was sent to a computer for data acquisition.

At elevated temperature the decay lifetime of the phosphorescence was recorded whilst the sample was in a furnace, as shown in Fig. 3. The excitation laser light was directed through an optical port in the furnace door using a single mirror. A non-imaging optical probe, described in detail elsewhere [8,10,23], was used to collect the phosphorescence. The probe was designed by Southside Thermal Sciences (STS) to have a uniform observation volume without a focal point to collect light into an optical fibre, eliminating the requirement for precise alignment. It has a wide acceptance angle and an opening aperture of 23 mm and was placed at a stand-off distance of approximately 450 mm from the sample. The observed light was then delivered, through the optical fibre, to a photo-multiplier tube (PMT) via a band pass filter, centred at 620 nm (Comar 620IL25). The PMT signal was amplified before being digitised and averaged with an oscilloscope (Tektronix DPO 3034). For each measurement, 30 decay recordings, which were the average of 10 individual decays, were fitted using the Nelder Mead Simplex method to an exponential of the form given in Eq. (3) including a constant offset term. The resultant decay time was taken as the mean of the decay times determined from the 30 fitted recordings.

4. Results and discussion

4.1. Influence of the dopant concentration in YSZ:Sm

4.1.1. Crystal structure

The XRD measurements recorded from the three YSZ:Sm powder materials with different concentrations of samarium are shown in Fig. 4. The $c/a\sqrt{2}$ ratio for all the XRD traces are shown in Table 1 along with values for an undoped YSZ. The ratio for the doped coatings was found to be approximately 1.01, and there are peaks at 73.5° and 74.2°, representing the lattice parameters $(0\,0\,4)_t$ and $(2\,2\,0)_t$ respectively. These peaks are characteristic of the

Table 1
Lattice parameters for increasing concentration of samaria in YSZ:Sm powders determined by Rietveld refinement. The error on the a, b and c values with the Rietveld method is ±0.0002.

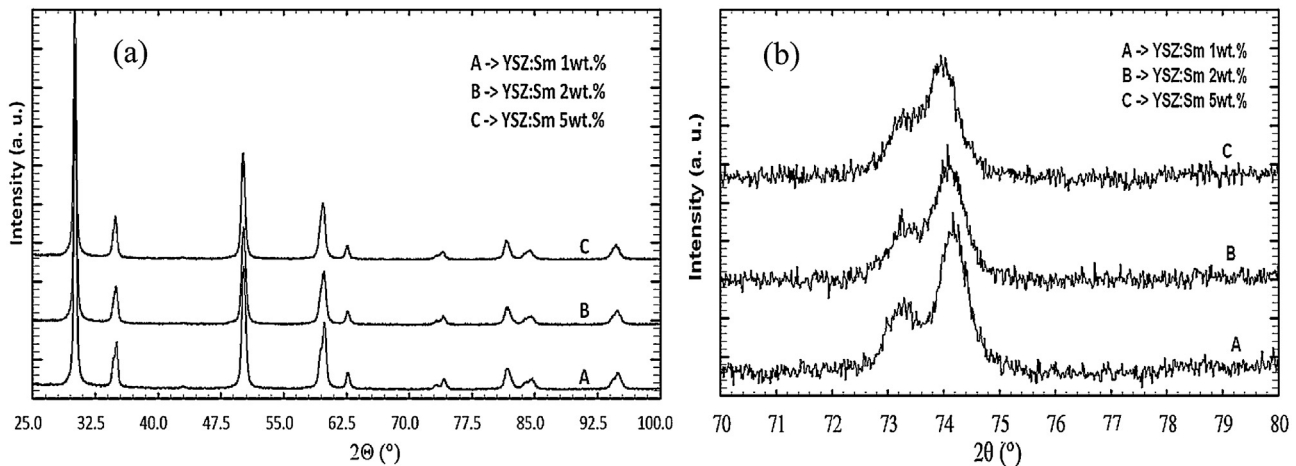| wt.% SmO$_{1.5}$	a and b (Å)	c (Å)	$c/a\sqrt{2}$
0	3.6219	5.1365	1.003
1	3.6208	5.1595	1.008
2	3.6172	5.1607	1.009
5	3.6143	5.1631	1.010

Fig. 4. The diffraction patterns of YSZ:Sm powder with increasing concentration of samarium (a) across the complete angular range and (b) covering only the 70–80° angular range.
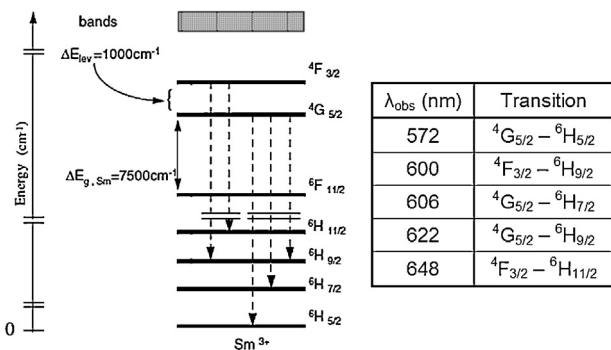

Fig. 5. The energy levels of trivalent samarium redrawn after [33], showing the radiative transitions and their respective wavelengths.

λ_{obs} (nm)	Transition
572	$^4G_{5/2} - {}^6H_{5/2}$
600	$^4F_{3/2} - {}^6H_{9/2}$
606	$^4G_{5/2} - {}^6H_{7/2}$
622	$^4G_{5/2} - {}^6H_{9/2}$
648	$^4F_{3/2} - {}^6H_{11/2}$

tetragonal phase. The XRD results, therefore, confirm that the synthesised materials were in the tetragonal phase. Furthermore, as the dopant concentration of samaria increases the peaks at 73.5° and 74.2° become closer together, indicating that the material tends towards a cubic structure [16,24].

4.1.2. Phosphorescence characteristics

The energy levels of trivalent samarium are shown in Fig. 5 along with the expected emission wavelengths. The emission spectra from each of the powder samples of YSZ:Sm with different dopant
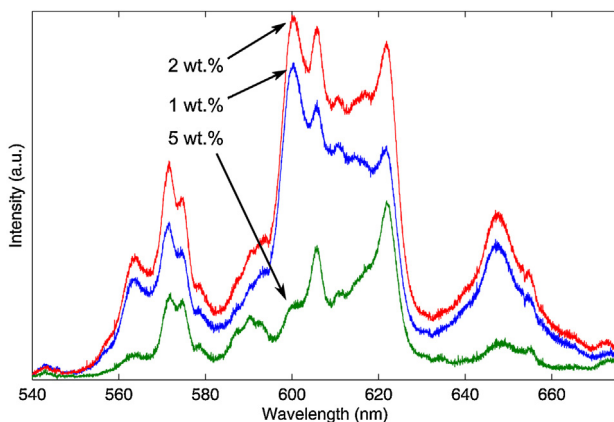

Fig. 6. The phosphorescence emission spectra from YSZ:Sm powder samples with three different dopant concentrations.

concentrations are shown in Fig. 6. The observed lines in the emission spectrum correspond with the expected emission lines from the energy level transitions given in Fig. 5.

There was a marked difference in the emission spectrum as the dopant concentration changes. The change in the intensity for each of the emission peaks is shown in Fig. 7. As the concentration increases from 1 wt.% to 5 wt.%. There was an increase in relative intensity at 572 nm and 606 nm with a particularly marked increase at 622 nm relating to the transition $^4G_{5/2}-{}^6H_{9/2}$. A significant suppression of intensity was observed at 600 and 648 nm.

The recorded emission spectrum was integrated between 560 nm and 670 nm for each sample to give an indication of the emission intensity. The plot is shown in Fig. 8. The maximum intensity was observed at 2 wt.% $SmO_{1.5}$ concentration. Below this value the intensity was limited by the number of dopant ions. Above this value concentration quenching occurs, whereby the dopant concentration is high enough that the dopant ions can interact with each other and as such can no longer be considered free ions. In this condition the energy can be passed between neighbouring ions increasing the probability of non-radiative transitions, reducing the
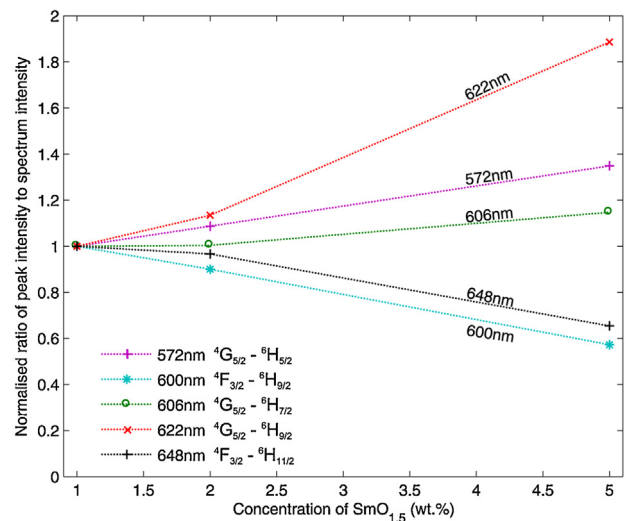

Fig. 7. The relative change in the intensity at the emission peaks as the dopant concentration increases is shown by plotting the ratio of the integrated intensity at each emission peak (1 nm bandwidth) to the integrated intensity of the full recorded spectrum (560–670 nm). The values are normalised at the value for 1 wt.% $SmO_{1.5}$ to depict the trends.
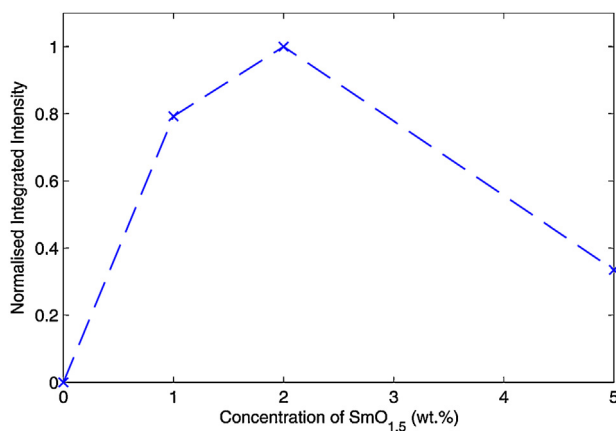
Fig. 8. The integration of the emission spectrum between 560 and 670 nm is plotted against the dopant concentration as a measure of the emission intensity.

Fig. 10. Phosphorescence emission spectrum of YSZ:Sm from a powder and coating sample, excited at 266 nm.

Fig. 11. The emission spectra from YSZ:Sm heat treated to different temperatures, normalised to the peak at 622 nm. A moving average filter with a sample width of 4 data points was applied to reduce the effect of noise on the normalisation.

quantum efficiency and emission intensity. These results indicate that the optimum dopant concentration of $SmO_{1.5}$ in YSZ in order to achieve the greatest intensity is approximately 2 wt.%.

4.2. Difference between YSZ:Sm powder and coating

4.2.1. Crystallinity

The diffraction patterns from the YSZ:Sm powder and coating with a surface layer of the same composition are shown in Fig. 9. The peaks in the diffraction of the YSZ:Sm powder were broader than those in the trace of the coating, representing a lower degree of crystallinity. This may be due to a difference in heat treatment temperature. The powder was heat treated at 950 °C whereas the coating was heat treated at 1100 °C. The XRD results indicate that the higher temperature of exposure of the coating caused a more complete crystallisation of the material.

4.2.2. Phosphorescence spectra

The emission spectrum from the coating with a top layer of YSZ:Sm was compared to the powder of the same composition. The spectra are shown in Fig. 10. The first observation to make is that the emission from the coating is significantly weaker compared to that from the powder. This is because there is less material to be excited in the thin YSZ:Sm coating layer compared to the powder sample. The second, more significant, observation is the difference in the relative intensity of the emission peaks, particularly at 600 nm and 648 nm. This suggests that the higher temperature exposure of
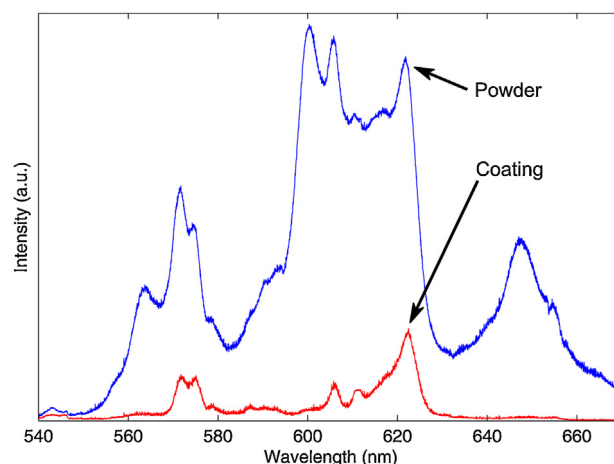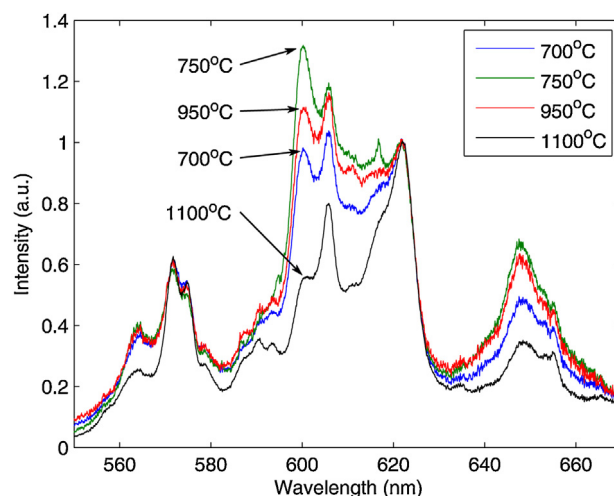
the coating, 1100 °C, compared to the powder, 950 °C, causes the suppression of particular radiative transitions.

The YSZ:Sm 2 wt.% powder batch which was heat treated to 700 °C was used to confirm this conclusion. Samples of the powder were heat treated for one hour at 750 °C, 950 °C and 1100 °C.
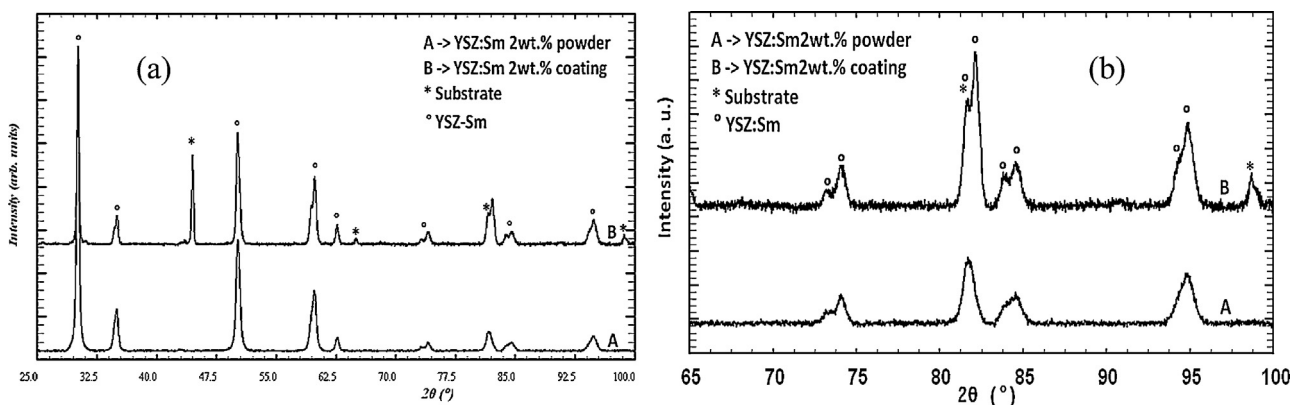

Fig. 9. The diffraction patterns of the YSZ:Sm powder and coating of the same composition (a) across the complete angular range and (b) covering only the 65–100° angular range.
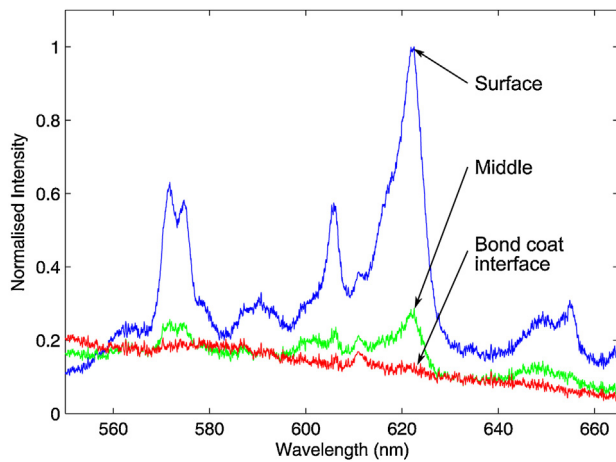
Fig. 12. The phosphorescence emission from the multi-layered coating samples shown in the schematic in Fig. 1. A moving average filter with a sample width of 4 data points was applied to reduce the amplitude of the noise.

The emission spectrum was recorded from each sample and the results are compared in Fig. 11. The spectra were normalised to the peak at 622 nm to clearly depict the relative changes in the other emission peaks. This peak was chosen because it is still present in the emission spectrum of the coating, as shown in Fig. 10. There was a clear change in the intensity of the emission at 600 nm and 648 nm for increasing thermal exposure. Increasing the heat treatment temperature from 700 °C to 750 °C caused the relative intensity at these wavelengths to increase to a maximum. The intensity remains higher than 700 °C for a heat treatment temperature of 950 °C. However, for the sample treated at 1100 °C, there was a significant relative reduction in intensity. This concurs with the comparison between the emission spectra of the powder and coating in Fig. 10. It is therefore concluded that the difference between the spectrum of the powder and coating of the same composition is due to subtle changes in the degree of crystallinity, identified in the XRD results, and due to the difference in heat treatment temperature. Heat treatment at 1100 °C appears to suppress the transitions from the $^4F_{3/2}$ level in favour of transitions from the $^4G_{5/2}$ level, similar to the effect of increasing the dopant concentration to 5 wt.%. A greater degree of crystallinity, therefore, may allow more interaction between dopant ions, similar to increasing the dopant concentration, which suppresses these transitions. It is expected that this behaviour would not be observed in materials produced via alternative methods which do not exhibit changes in crystallinity. This observation suggests that YSZ:Sm produced via sol–gel could be used as a thermal history sensor, similar to those reported in the literature [25–27]. This is the first indication that YSZ, the industry standard material for TBCs, could be used as the sensing material for thermal history applications.

4.3. Multi-layered coatings

The phosphorescence emission was recorded from each of the multi-layered coating constructions to investigate the effect of embedding the dopant layer on the phosphorescence signal. The results are shown in Fig. 12. The phosphorescence signal, clearly visible when the doped layer was at the surface, remains detectable underneath a 50 μm layer of undoped YSZ. In this case, however, it was not possible to detect the phosphorescence when the overcoat YSZ layer was 100 μm thick. The attenuation of the phosphorescence signal due to the YSZ overcoat is expected. This is because although YSZ is translucent in the visible range the excitation wavelength, 266 nm, is approaching the band gap of YSZ at approximately 215 nm [28]. Therefore, a significant proportion of
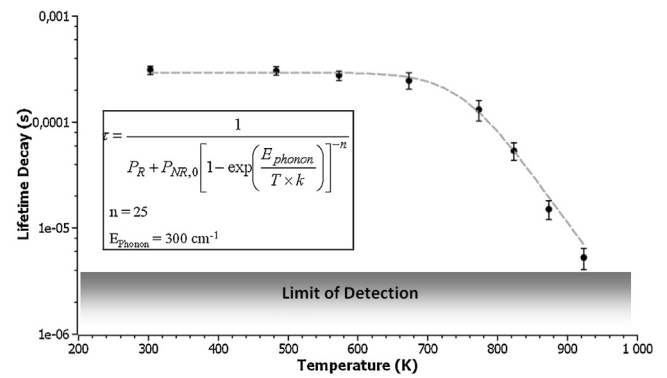

Fig. 13. The lifetime decay versus temperature for YSZ:Sm with 2 wt.% SmO$_{1.5}$. The excitation and observation wavelength is 266 nm and 620 nm respectively.

the excitation light will be absorbed. In addition, both the excitation and emission light will be scattered through the YSZ layer.

The detection of the phosphorescence from a relatively thin, 20 μm, layer either at the surface or beneath a 50 μm YSZ overcoat indicates that doped YSZ could be applied either as a thin film or as a subsurface layer with an overcoat of undoped YSZ. As such this technique can be used to produce sensor TBCs for a range of possible application areas.

4.4. On-line temperature detection

The decay time of the phosphorescence of the YSZ:Sm 2 wt.% powder was recorded with increasing temperature. The band pass filter is centred at 620 nm and has a bandwidth at half maximum of 10 nm, therefore the $^4G_{5/2}$–$^6H_{9/2}$ transition was observed. The results, plotted in Fig. 13, show that at lower temperatures, up to approximately 400 °C, the decay value stayed relatively constant. Above this temperature, also called the quenching temperature, there was significant thermal quenching of the phosphorescence and the decay time decreases. It was not possible to record a measurement above 700 °C because the signal becomes too weak for detection.

By substitution of Eq. (3) into Eq. (2) an equation is formed which describes the change in lifetime decay with temperature according to the multi-phonon relaxation model. The experimental results were fitted with this equation using a commercial data processing routine based on the Nelder–Mead Simplex algorithm. The energy gap between the lowest radiative and highest non-radiative energy level, which is required to be bridged for non-radiative decay to occur, is assumed to be unaffected by the host and hence is 7500 cm^{-1} according to Fig. 5. The resultant fit, shown as a solid line in Fig. 13, provides a close match to the experimental data and a value for the phonon energy of 300 cm^{-1}. Given this phonon energy, this model states that the simultaneous release of 25 phonons are required to cause non-radiative decay. The high order of the process is comparable to previous findings [6,18]. This value is, however, above the rule of thumb for rare earth ions which states that if over seven phonons are required then the dominant decay mechanism is radiative [29]. Even with the maximum phonon energy possible for YSZ, 685 cm^{-1} [30], 11 phonons are required to bridge the energy gap.

An alternative description of the temperature dependence of phosphorescence decay was proposed by Fonger and Struck [31] and it has been applied to rare earth doped material with a similar temperature range to that shown here for YSZ:Sm [32]. The increasing decay rates at high temperatures are attributed to thermally activated non-radiative decay pathways through the charge transfer state. The alternative description can be used to prescribe a different decay mechanism for YSZ:Sm whereby the laser light

at 266 nm causes excitation of a charge transfer state which fills the $^4F_{3/2}$ and $^4G_{5/2}$ levels. From here the relaxation occurs either through radiative transitions to the H levels or, at high temperature, the thermal energy allows the electron to return to the charge transfer state which facilitates further non-radiative transition to the H levels. This decay route offers an explanation for how the large energy gap may be overcome without the release of a large number of phonons.

It is likely that a combination of multi-phonon relaxation and the charge transfer state relaxation causes the temperature dependence of the YSZ:Sm. Further investigation into the different energy level transitions would be required to offer a complete explanation of the decay pathways however this is outside the scope of the current investigation.

Although the temperature range of the YSZ:Sm is too low for advanced gas turbine applications it could be used in lower temperature regimes. Alternative dopant materials could be used to produce sensor TBCs with a higher temperature sensitivity range. Furthermore, since it has been established that a phosphorescence signal has been detected from the material, either in powder or coating form, the sol–gel process could be used to produce material or apply coatings for use in a health monitoring capacity. This approach can make use of the known capability of phosphorescence materials for detection of phase changes, chemical attack or erosion [5].

5. Conclusion

YSZ powders and coatings doped with samaria have been successfully synthesised by a sol–gel process. It was possible to detect the phosphorescence from these materials demonstrating that it is possible to manufacture sensor TBCs through the sol–gel process. By producing and testing powders with different concentrations of dopant it has been shown that the optimum concentration of $SmO_{1.5}$ in YSZ is approximately 2 wt.% for maximum phosphorescence intensity. Further, increasing the dopant concentration above this optimum level causes distortion of the crystalline structure and the material tends towards the undesirable cubic phase. These distortions are reflected in the phosphorescence emission spectrum and confirmed by XRD analysis.

The XRD measurements indicate that the temperature of heat treatment of the YSZ:Sm has an effect on the degree of crystallisation of the material. This was further corroborated by analysis of the phosphorescence from powder samples calcinated at 700, 750, 950 and 1100 °C, which exhibit different emission spectra. The thermal exposure has a significant effect on the intensity of the emission at 600 and 648 nm, relating to the $^4F_{3/2}$ to either $^6H_{9/2}$ or $^6H_{11/2}$ transitions. This observation indicates, for the first time, that it is possible to produce YSZ so that it can be used as a thermal history sensor.

Layered ceramic coatings, produced by dip coating, have shown that the phosphorescence can be detected from thin layers, 20 μm thick, even when underneath a 50 μm thick layer of undoped YSZ. Furthermore, it has been shown that the temperature sensitivity range of the YSZ:Sm is between 400 and 700 °C. The combination of the detection of phosphorescence from thin layers and the temperature sensitivity range demonstrate that this material and production method have potential for low temperature regimes. Alternatively this production method could be used to deposit sensor materials for health monitoring purposes.

Acknowledgements

References

[1] A.K. Gupta, Gas turbine combustion: prospects and challenges, Energy Conversion and Management 38 (1997) 1311–1318.

[2] A. Poullikkas, An overview of current and future sustainable gas turbine technologies, Renewable and Sustainable Energy Reviews 9 (2005) 409–443.

[3] R. Kehlhofer, B. Rukes, F. Hannemann, F. Stirnimann, Combined-Cycle Gas & Steam Turbine Power Plants, Pennwell Books, USA, 2009, ISBN 978-1-59370-168-0.

[4] M. Madhwal, E.H. Jordan, M. Gell, Failure mechanisms of dense vertically-cracked thermal barrier coatings, Materials Science and Engineering A 384 (2004) 151–161.

[5] K.L. Choy, A. Heyes, J. Feist, Thermal Barrier Coating with Thermoluminescent Indicator Material Embedded Therein, WO Patent WO/2000/006,7962000.

[6] R. Steenbakker, J. Feist, R. Wellman, J. Nicholls, Sensor thermal barrier coatings: remote in situ condition monitoring of EB-PVD coatings at elevated temperatures, Journal of Engineering for Gas Turbines and Power 131 (2009) 041301.

[7] J.I. Eldridge, T.J. Bencic, S.W. Allison, D.L. Beshears, Depth-penetrating temperature measurements of thermal barrier coatings incorporating thermographic phosphors, Journal of Thermal Spray Technology 13 (2004) 44–50.

[8] J.P. Feist, P.Y. Sollazzo, S. Berthier, B. Charnley, J. Wells, Precision temperature detection using a phosphorescence sensor coating system on a Rolls-Royce Viper engine, Paper No. GT2012-69779, in: Proceedings of the ASME Turbo Expo, Copenhagen, Denmark, 2012.

[9] J. Feist, P. Sollazzo, S. Berthier, B. Charnley, J. Wells, Application of an industrial sensor coating system on a Rolls-Royce jet engine for temperature detection, Journal of Engineering for Gas Turbines and Power 135 (2013) 012101.

[10] J.P. Feist, P.Y. Sollazzo, S. Berthier, B. Charnley, J. Wells, Application of an industrial sensor coating system on a Rolls-Royce jet engine for temperature detection, in: Proceedings of the 6th Conference of the Institute of Diesel and Gas Turbine Engineers IDGTE, Milton Keynes, UK, 2011.

[11] http://www.youtube.com/watch?v=_jLWNkYYr8U&feature=plcp, Phosphorescence sensor coating for online temperature detection, 2011.

[12] N.P. Padture, M. Gell, E.H. Jordan, Thermal barrier coatings for gas-turbine engine applications, Science 296 (2002) 280–284.

[13] X. Chen, Z. Mutasim, J. Price, J. Feist, A. Heyes, S. Seefeldt, Industrial Sensor TBCs: studies on temperature detection and durability, International Journal of Applied Ceramic Technology 2 (2005) 414–421.

[14] J. Sniezewski, Y. Le Maoult, P. Lours, L. Pin, V.M. Bekale, D. Monceau, et al., Sol–gel thermal barrier coatings: optimization of the manufacturing route and durability under cyclic oxidation, Thin Solid Films 205 (5) (2010) 1256–1261.

[15] J. Fenech, C. Viazzi, J.P. Bonino, F. Ansart, A. Barnabé, Morphology and structure of YSZ powders: comparison between xerogel and aerogel, Ceramics International 35 (2009) 3427–3433.

[16] C. Viazzi, J.P. Bonino, F. Ansart, A. Barnabé, Structural study of metastable tetragonal YSZ powders produced via a sol–gel route, Journal of Alloys and Compounds 452 (2008) 377–383.

[17] L. Pin, F. Ansart, J.P. Bonino, Y. Le Maoult, V. Vidal, P. Lours, Reinforced sol–gel thermal barrier coatings and their cyclic oxidation life, Journal of the European Ceramic Society 33 (2) (2013) 269–276.

[18] A. Heyes, On the design of phosphors for high-temperature thermometry, Journal of Luminescence 129 (2009) 2004–2009.

[19] A.H. Khalid, K. Kontis, Thermographic phosphors for high temperature measurements: principles, current state of the art and recent applications, Sensors 8 (2008) 5673–5744.

[20] M.J. Weber, Radiative and multiphonon relaxation of rare-earth ions in Y_2O_3, Physical Review 171 (1968) 283–291.

[21] M. Shane, M. Mecartney, Sol–gel synthesis of zirconia barrier coatings, Journal of Materials Science 25 (1990) 1537–1544.

[22] H.M. Rietveld, A profile refinement method for nuclear and magnetic structures, Journal of Applied Crystallography 2 (1969) 65–71.

[23] J.P. Feist, S. Zhang, Optical Probe and Apparatus, Southside Thermal Sciences, UK, 2010.

[24] S. Tsipas, Effect of dopants on the phase stability of zirconia-based plasma sprayed thermal barrier coatings, Journal of the European Ceramic Society 30 (2010) 61–72.

[25] J. Feist, J. Nicholls, A.L. Heyes, Determining thermal history of components, patent number WO/2009/083, 2007, p. 729.

[26] A. Rabhiou, J. Feist, A. Kempf, S. Skinner, A. Heyes, Rare earth ceramic phosphorescent thermal history sensors, Sensors and Actuators A: Physical 169 (2011) 18–26.

[27] A.L. Heyes, A. Rabhiou, J.P. Feist, A.M. Kempf, Phosphor based temperature indicating paints, paper no. GT2012-69811, in: Proceedings of Asme Turbo Expo 2012, Copenhagen, Denmark, 2012.

[28] N. Nicoloso, A. Lobert, B. Leibold, Optical absorption studies of tetragonal and cubic thin-film yttria-stabilized zirconia, Sensors and Actuators B: Chemical 8 (1992) 253–256.

[29] B. Di Bartolo, J. Collins, Luminescence spectroscopy, in: D. Vij (Ed.), Handbook of Applied Solid State Spectroscopy, Springer, 2006, pp. 509–575.

[30] B. Savoini, J.E.M. Santiuste, R. Gonzalez, Optical characterization of Pr^{3+}-doped yttria-stabilized zirconia single crystals, Physical Review B 56 (1997) 5856.

[31] W. Fonger, C. Struck, $Eu + {}^{35}D$ resonance quenching to the charge-transfer states in Y_2O_2S, La_2O_2S, and $LaOCl$, Journal of Chemical Physics 52 (1970) 6364–6372.

[32] M. Chambers, P. Rousseve, D. Clarke, Decay pathway and high-temperature luminescence of Eu^{3+} in $Ca_2Gd_8Si_6O_{26}$, Journal of Luminescence 129 (2009) 263–269.

[33] J. Feist, A. Heyes, The characterization of Y_2O_2S: Sm powder as a thermographic phosphor for high temperature applications, Measurement Science and Technology 11 (2000) 942.

Biographies

Lisa Pin Doctor in Materials Science since 2012 – Research Engineer Safran Herakles, Le Haillan – France. Fields of interest: sol–gel route, high temperature coating, ceramic.

Christopher Pilgrim After completing a Master's degree in Materials and Mechanical Engineering, Christopher Pilgrim joined Sensor Coating Systems, as part of the engineering doctorate scheme. The programme is coordinated by the Research Centre for Non-Destructive Evaluation and supported by the EPSRC. During this time he has worked on all development projects for the company, developing the Thermal History Coating technology as well as playing a prominent role in the erosion sensor development. In addition, he has been heavily involved in the design, construction and operation of STS test facilities, conducting tests for large commercial clients in both power generation and aerospace industries.

Jörg Feist Jörg is responsible for general management, research and technical development at Sensor Coating Systems. He is co-inventor of the sensor technology. Jörg has a PhD in Mechanical Engineering from Imperial College London and a first degree in Physics from the University Duisburg-Essen, Germany. Jörg has driven the SCS programme from foundation of the company to the present day. He was responsible for successfully delivering various EU and UK co-funded projects often with international participation. Further, he successfully delivered commercially funded R&D projects for the automotive and gas turbine industry. He is the co-author of more than 40 technical papers and several patents and patent applications, covering the areas of thermographic phosphors thermal barrier coatings, engine diagnostic and optics.

Yannick Le Maoult After a PhD in physics obtained in Marseille in 1992 (Université de Provence) related to infrared radiometry applied to combustion science, Dr Yannick Le Maoult joined the Ecole des Mines d'Albi in 1995 as an associate professor. He has founded the LAMIR (Laboratory dedicated to infrared physic applications, thermal science and measurements) in Ecole des Mines d'Albi (ICA-A). Dr Y. Le Maoult is currently a full professor in Ecole des Mines d'Albi and he supervises research in the area of radiative transfer, optical properties of materials, infrared measurements and luminescence problems.

Florence Ansart Doctor engineer in Materials Science since 1992 Professor of University since 2005, Toulouse – France Fields of interest: Sol–gel route, ceramics, synthesis and processing of protective and functional coatings, microstructure.

Philippe Lours Materials Science and Engineering, high temperature alloys, coatings Professor Post-Doctoral Fellow Lawrence Berkeley Laboratory (1990) PhD University of Toulouse (1986) Master Degree in Solid State Physics (1986).